Spectrochimica Acta Part A: Molecular and Biomolecular Spectroscopy 172 (2017) 189–198

Contents lists available at ScienceDirect

Spectrochimica Acta Part A: Molecular and Biomolecular Spectroscopy

journal homepage: www.elsevier.com/locate/saa

Synthesis, structural and spectroscopic studies of 2-oxoacenaphthylen-1(2*H*)-ylidene nicotinohydrazide

M.S.C. Henriques [a], R. Del Amparo [b], D. Pérez-Álvarez [b], B.A. Nogueira [c], M.C. Rodríguez-Argüelles [b], J.A. Paixão [a,*]

[a] CFisUC, Department of Physics, University of Coimbra, P-3004-516, Coimbra, Portugal
[b] Departamento de Química Inorgánica, Universidade de Vigo, 36310 Vigo, Spain
[c] Department of Chemistry, University of Coimbra, P-3004-535, Coimbra, Portugal

ARTICLE INFO

Article history:
Received 13 November 2015
Received in revised form 12 February 2016
Accepted 15 February 2016
Available online 19 February 2016

Keywords:
Acylhydrazone
Polymorphism
XRD
Ab-initio calculations
FT-IR
Raman

ABSTRACT

The synthesis of a new hydrazone, 2-oxoacenaphthylen-1(2*H*)-ylidene nicotinohydrazide, and its structural and spectroscopic characterization is reported. The obtained powder was recrystallized from DMSO and ethanol that afforded small crystals used for single-crystal X-ray diffraction studies. The compound was found to crystallize in two polymorphs, depending on the crystallization conditions. One of the polymorphs (form I) crystallizes in the centrosymmetric $P2_1/c$ monoclinic space group, the other (form II) crystallizes in the non-centrosymmetric, but achiral, orthorhombic space group $P2_12_12_1$. Conformation of the molecules is similar in both polymorphs, but the network of weak intermolecular interactions determining the crystal packing is different. In form II an additional C–H···O bond connects molecules related by the screw-axis running parallel to the *a*-axis. Crystals of both polymorphs were also screened by FT-IR and Raman microscopy; a detailed analysis of the spectra and comparison with those of the isolated molecule calculated by *ab-initio* HF/MP2 and DFT/B3LYP methods using a correlation consistent cc-pVDZ basis set is presented. In addition, UV–vis and NMR studies were performed in solution.

1. Introduction

Acylhydrazones are very versatile compounds that offer a wide range of applications in different fields including catalysis, supramolecular chemistry and biology [1]. One should highlight anti-inflammatory, analgesic, antipyretic, antimicrobial, vasodilatory, antipsychotical, antimalarial and antitumoral activities [1–4]. In addition, acylhydrazones feature donor atoms in the central skeleton that, together with potential donor atoms of the –R groups, can lead to a high coordinative versatility. Another relevant factor is the presence of keto-enol tautomerism, where each tautomer can present different resonance (*E*/*Z*) forms [5,6], as shown in Fig. 1.

In this work we present the synthesis of a new acylhydrazone, by reaction of nicotinic hydrazide with acenaphthenequinone, the latter having been chosen for its high antitumor potential [7]. While attempting to use the new compound as chelating agent of transition metal atoms, to further improve its pharmacological potential, it was found to crystallize in two distinct polymorphic forms. A thorough study of these polymorphs using X-ray diffraction (XRD), spectroscopy techniques in solid state (FT-IR and Raman) and solution (UV–vis and NMR), and *ab-initio* calculations aiming at characterizing the molecular conformation and crystal packing were undertaken and presented in this paper.

2. Materials and methods

All reagents were obtained from commercial sources and used without further purification. Acenaphthenequinone and nicotinic hydrazide (97%) were purchased from Aldrich, acetic acid (99.5%) was purchased from Poch and absolute ethanol (99.5%) from Panreac.

2.1. Analytical instruments and spectroscopy techniques

Elemental analyses were performed on a Carlo Erba 1108 elemental analyzer. Melting points were determined on a Gallen Kamp MDP350.BM2.5 instrument. Crystals of the two polymorphs were examined on a Thermo Nicolet iN10 MX IR microscope. IR spectra were collected in ATR (Ge tip) mode, using a LN2 cooled MCT detector, covering the range 650–4000 cm^{-1} with a resolution of 4 cm^{-1}. Additional FT-IR measurements, recorded in KBr pellets on a Jasco FT/IR-6100 spectrometer are given in supplementary material. Raman data were collected on a Horiba LabRam HR Evolution Raman microscope in the wavenumber range 350–4000 cm^{-1} using an exciting wavelength of 633 nm (HeNe laser) and a Synapse CCD detector (resolution of 1.5 cm^{-1}/pixel). NMR data were measured on a Bruker AVANCE DPX-400 spectrometer, in DMSO-d_6 solutions. UV–vis absorption spectra of the compound were measured in CH_3CN, at

* Corresponding author.
E-mail address: jap@fis.uc.pt (J.A. Paixão).

http://dx.doi.org/10.1016/j.saa.2016.02.012
1386-1425/

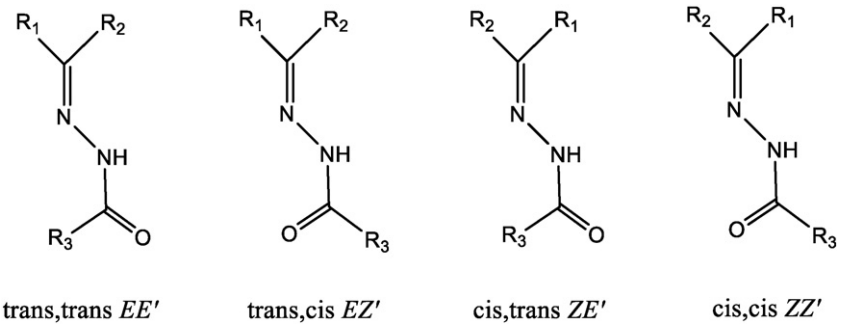

Fig. 1. Different *E*, *Z* isomers of acylhydrazones.

room temperature, on a Jasco V-670 spectrometer, in the wavelength range of 200–800 nm.

2.2. Synthesis

2-oxoacenaphthylen-1(2*H*)-ylidene nicotinohydrazide was synthesized by a condensation reaction [8], and detailed as follows. To a solution of acenaphthenequinone (8.7 mmol) in 40 mL ethanol was added 5 mL of acetic acid 99.5%. Then, nicotinic hydrazide (8.7 mmol) previously dissolved in 25 mL distilled water was slowly added. The reaction mixture was stirred and refluxed for 24 h at 70 °C. After cooling, the yellow solid product was vacuum filtered, washed several times with ethanol and dried. Yield 81%; m.p.: 201 °C. Anal. Exp.: C, 71.83; H, 3.78; N, 13.89%. Calc. for $C_{18}H_{11}N_3O_2$: C, 71.75; H, 3.68; N, 13.95%.

Small single crystals suitable for X-ray diffraction studies were obtained by slow evaporation over several weeks in DMSO, at room temperature, and ethanol, slowly cooling from a pre-heated solution in ethanol at 60 °C. These were latter confirmed by XRD as two distinct polymorphs that we label polymorph I (DMSO) and polymorph II (ethanol).

Table 1
Crystal data and XRD structure refinement details.

	Form I	Form II
Empirical formula	$C_{18}H_{11}N_3O_2$	$C_{18}H_{11}N_3O_2$
Formula weight	301.30	301.30
Crystal system	Monoclinic	Orthorhombic
Space group	$P2_1/c$	$P2_12_12_1$
a(Å)	8.6333(6)	3.9447(2)
b(Å)	12.4198(8)	16.0233(8)
c(Å)	13.7430(9)	21.8386(11)
α(°)	90	90
β(°)	109.503(4)	90
γ(°)	90	90
Volume	1389.03(16)	1380.35(12)
Z	4	4
D_{calc}	1.441	1.450
μ	0.097	0.098
F_{000}	624	624
hkl range	−10,10; −14,14; −16,16	−4,4; −18,18; −25,25
θrange(°)	2.277–24.999	2.257–24.989
Measured reflections	2444	2428
Observed reflections	1484	1568
Number of refined parameters	209	209
R_{int}	0.0706	0.1049
R_1	0.0444	0.0459
wR_2	0.1161	0.1158
GOF in F^2	1.028	1.015
Residual density	−0.157, 0.170	−0.140, 0.209

2.3. Single-crystal X-ray crystallography

The crystal structures of the two polymorphs were determined by single-crystal X-ray diffraction. The data were collected at room temperature on a Bruker APEX II X-ray diffractometer equipped with a 4 K CCD detector, using graphite monochromatized Mo (K_α radiation λ = 0.71073 Å). Crystals were attached on top of a glass-fiber with a small amount of perfluoropolyether vacuum oil. Integration of frames and scaling of data was performed using the SAINT [9] suite of programs. Empirical absorption correction was applied to all data using SADABS

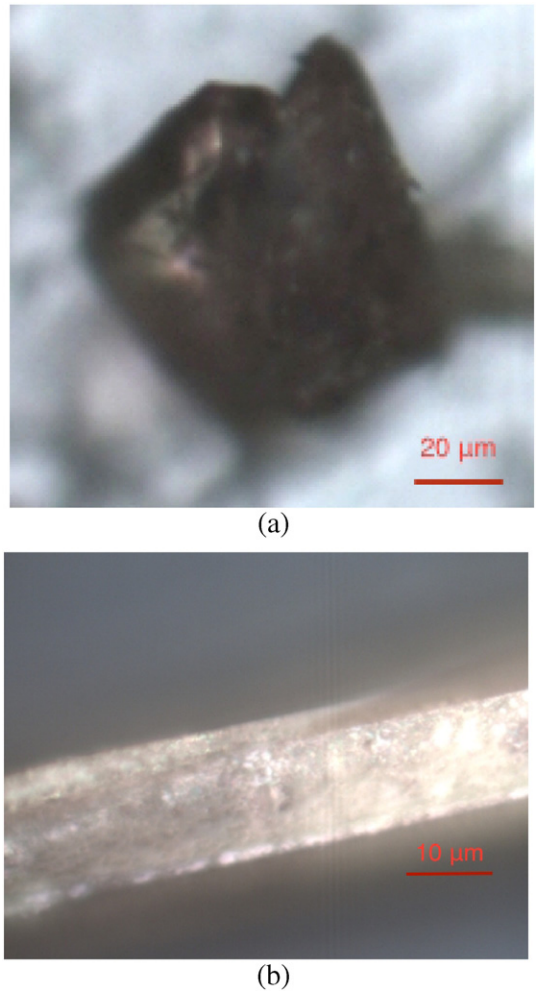

Fig. 2. Images of crystals of polymorphs I (a) and II (b).

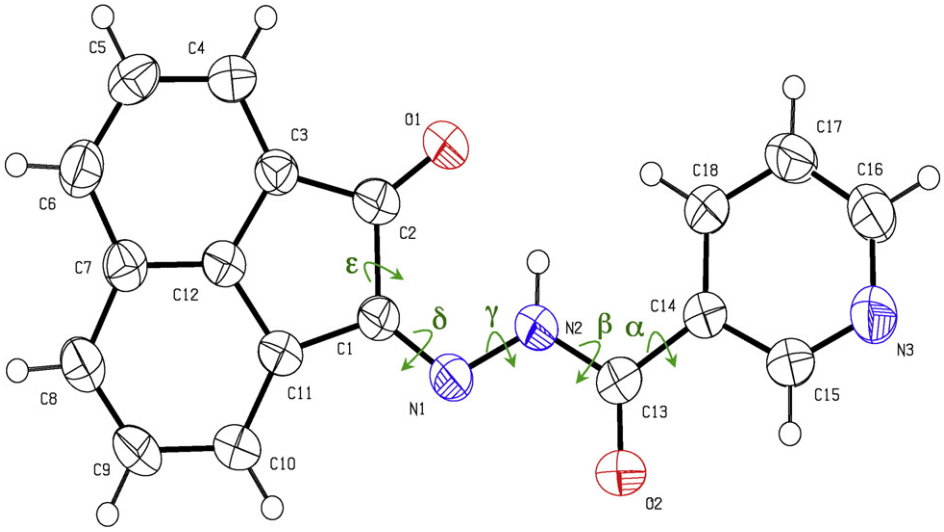

Fig. 3. ORTEP plot showing the atom numbering scheme (polymorph I). Anisotropic displacement ellipsoids are drawn at the 50% probability level. The torsion angles α…ε are used to describe the internal rotational degrees of freedom of the molecule.

[9]. Structure solution was performed by direct methods using SHELXT-2014/4 [10]. Structural refinement was performed by full matrix least-squares using SHELXL-2014/7 [11]. All atoms, except H, were refined anisotropically. H atoms were refined as riding on top of their parent atoms using SHELXL-2014 default values. Details of the crystal structures, data collection and refinement for the two polymorphs are summarized in Table 1. Crystallographic figures and tables were produced using PLATON [12]. CCDC 1411972 (polymorph I) and CCDC 1411973 (polymorph II) contain supplementary crystallographic data.

2.4. Ab-initio and DFT calculations

Optimization of the geometry of the isolated molecule was performed with Hartree–Fock (HF), HF/MP2 and DFT/B3LYP methods, starting from the XRD geometry, using a sequence of basis sets: 3-21G, 6-31G(d,p) and Dunning's correlation consistent cc-pVDZ [13] (for MP2 and DFT methods). The calculations were performed using GAMESS [14] running on 10 nodes (240 processors) of the Navigator computing cluster of LCA-UC. The optimized structural parameters were used in the vibrational frequency calculations performed with both HF/MP2 and DFT/B3LYP with a correlation consistent cc-pVDZ basis set [13], resulting in IR and Raman frequencies along with intensities and Raman depolarization ratios. As it is well known that both HF and DFT hybrid B3LYP functional methods tend to overestimate the frequencies of fundamental modes due to shortcomings of the applied methodology, mainly related to anharmonicity, the scaling factors of 0.970 and 0.953 were uniformly applied to the frequencies calculated by DFT/B3LYP and HF/MP2 methods (cc-pVDZ basis set), respectively [15].

Calculation of the most intense UV–vis transitions to compare with experimental data measured in an acetonitrile solution was performed by TDDFT using GAMESS with the same settings as for the other calculations. Solvent effects were taken into account in the calculation with the C-PCM/SMD model [16].

Table 2
Bond distances (Å) determined from single-crystal XRD for polymorphs I and II.

	Form I	Form II	Calc.
O1–C2	1.228(3)	1.232(4)	1.231
O2–C13	1.211(3)	1.222(5)	1.215
N1–C1	1.288(3)	1.293(4)	1.299
N1–N2	1.367(2)	1.382(4)	1.339
N2–C13	1.368(3)	1.371(5)	1.399
N3–C16	1.331(3)	1.337(5)	1.342
N3–C15	1.334(3)	1.332(5)	1.337
C1–C11	1.462(3)	1.469(5)	1.471
C1–C2	1.513(3)	1.506(5)	1.515
C2–C3	1.464(3)	1.455(5)	1.485
C3–C4	1.373(3)	1.376(5)	1.383
C3–C12	1.402(3)	1.406(4)	1.417
C4–C5	1.396(3)	1.398(6)	1.420
C5–C6	1.377(3)	1.373(5)	1.392
C6–C7	1.409(3)	1.406(6)	1.424
C7–C12	1.403(3)	1.399(5)	1.411
C7–C8	1.417(3)	1.413(5)	1.427
C8–C9	1.362(3)	1.363(5)	1.387
C9–C10	1.419(3)	1.412(5)	1.425
C10–C11	1.366(3)	1.364(5)	1.381
C11–C12	1.414(3)	1.403(5)	1.421
C13–C14	1.484(3)	1.483(5)	1.501
C14–C15	1.377(3)	1.376(5)	1.407
C14–C18	1.383(3)	1.390(5)	1.403
C16–C17	1.364(3)	1.375(6)	1.398
C17–C18	1.369(3)	1.369(6)	1.395

3. Results and discussion

Elemental analysis shown in the previous section confirmed the high purity of the new acylhydrazone obtained under conventional

Table 3
Selected bond angles (Å) determined from single-crystal XRD for polymorphs I and II.

	Form I	Form II
C4–C3–C12	120.0(2)	119.9(3)
C3–C4–C5	117.5(2)	118.3(4)
C6–C5–C4	122.9(2)	121.6(4)
C5–C6–C7	120.7(2)	121.7(4)
C12–C7–C6	115.6(2)	115.9(3)
C12–C7–C8	116.1(2)	115.5(3)
C9–C8–C7	120.0(2)	119.9(4)
C8–C9–C10	123.3(2)	123.8(4)
C11–C10–C9	118.2(2)	117.4(4)
C10–C11–C12	118.8(2)	119.1(3)
C3–C12–C7	123.2(2)	122.5(3)
C7–C12–C11	123.7(2)	124.3(3)

Table 4
Molecular conformation in the two crystal forms and of the free molecule as given by *ab-initio* HF and DFT calculations.

	Form I (XRD)	Form II (XRD)	HF/6-31G(d,p)	HF/cc-pVDZ/MP2	DFT/cc-pVDZ
$\alpha(^{\circ})$	−1.49	10.80	20.5	21.4	14.0
$\beta(^{\circ})$	−0.23	7.79	3.0	3.7	3.7
$\gamma(^{\circ})$	173.56	177.28	−177.2	−178.8	−179.0
$\delta(^{\circ})$	−177.05	−175.64	−179.7	−0.6	−179.8
$\varepsilon(^{\circ})$	6.90	3.74	0.1	0.6	0.4
C1═N1 (Å)	1.288	1.293	1.260	1.314	1.299
C13═O2 (Å)	1.211	1.222	1.192	1.219	1.215
C2═O1 (Å)	1.228	1.233	1.198	1.237	1.231

heating conditions and a high yield of the reaction was achieved. The compound is soluble at room temperature in common organic solvents such as DMSO, dmf, $CHCl_3$ and CH_2Cl_2, features a lower solubility in ethanol, tetrahydrofuran and CH_3CN, and an extremely low solubility in water.

3.1. X-ray crystallography

Inspection of the crystals under an optical microscope showed the formation of crystals of different habits, and slightly different yellowish colors. The darker crystals had a prismatic form, often growing as clusters or "twins" (Fig. 2a), the lighter color crystals grow as thin needles (Fig. 2b). The XRD analysis of single-crystals of each crystal habit confirmed the existence of two polymorphs, a monoclinic and an orthorhombic form. Each crystal structure contains one unique molecule in the unit cell (both polymorphs feature 4 symmetry related molecules per unit cell). An ORTEP plot of the molecule with the atom labeling scheme is shown in Fig. 3.

Bond distances (Table 2) and angles (Table 3) in the molecules of the two polymorphs are similar in the two compounds and compare well with values reported in the literature for similar compounds [17–19]. The bonds distances C1–N1 and N2–C13 are consistent with their double and single bond character, respectively. Bond lengths and angles within the aromatic rings are in the expected range of values for sp^2 hybridization of the C atoms. The endocyclic angles of the naphthalen rings show significant deviations from the ideal values of 120°, but the molecule retains approximately the mirror plane perpendicular to the plane of the molecule running through the middle C7–C12 bond.

The acenaphthenequinone moiety is planar, the *rms* deviation from the least-squares plane of the molecule being less than 0.025 Å in both polymorphs, the carbonyl O1 atom lying in the plane but with the azomethine N1 atom slightly out of the plane [0.22 Å (I), 0.15 Å (II)]. The pyridyl ring and the N2–C13═O2–C14 group are also planar within 0.005 Å in both polymorphs. The acenaphthenequinone and pyridyl rings make an angle of 15.70(11)° and 16.09(14)° in polymorphs I and II, respectively. The angle between the N2–C13═O2–C14 group of atoms and the pyridyl rings are 2.30(16)° (I) and 10.09(14)° (II). Clearly, the molecule shows a certain degree of conformational flexibility that is given by the torsion angles α, β, γ, δ and ε as shown in Fig. 3. The experimental torsion angles determined from the XRD data are shown in Table 4. Most notably, the α and β torsion angles differ significantly from zero and are also quite different in the two polymorphs. The values of these torsion angles in the crystals are determined by steric, intra and intermolecular interactions. A survey of short contact distances indicates the presence of one strong intramolecular hydrogen bond between the NH group acting as proton donor and the acenaphthenequinone carbonyl O1 atom, as acceptor (Table 5). This intramolecular bond is found in the two polymorphs and in other acenaphthenequinone derivatives [19]. It stabilizes the *E* tautomeric form in the crystalline state. Another intramolecular short contact occurs between the C15–H and O2 atoms that could be classified as a weak hydrogen bond of the C–H type. Polymorph II features, in addition, an intermolecular C4–H4···O1 hydrogen bond interaction that connects neighbor molecules related by the 2_1 screw-axis running parallel to the crystallographic *a* axis. The crystal

Table 5
Hydrogen-bonding distances (Å) and angles (°).

Form	Atoms	D–H	H···A	D···A	D–H···A
I	N2—H2···O1	0.86	2.00	2.699(2)	137.4
I	C15—H15···O2	0.93	2.45	2.795(4)	101.6
II	N2—H2···O1	0.86	1.99	2.691(4)	137.7
II	C4—H4···O1^{i}	0.93	2.48	3.218(5)	136.6
II	C15—H15···O2	0.93	2.48	2.807(6)	101.0

$i = -1/2 + x, 1/2 - y, -z$

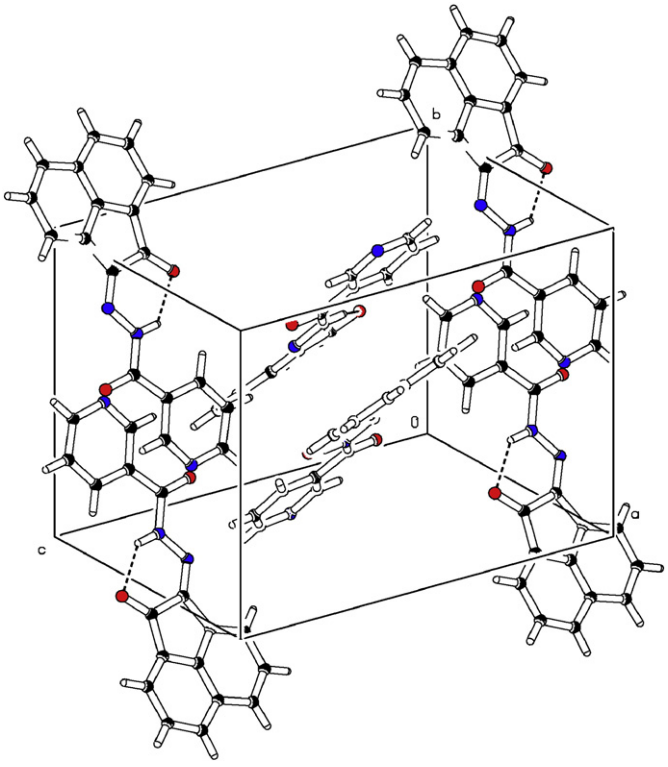

Fig. 4. Packing diagram of the molecules of polymorph I in the crystallographic unit cell. The intramolecular hydrogen bond is shown as a dotted line.

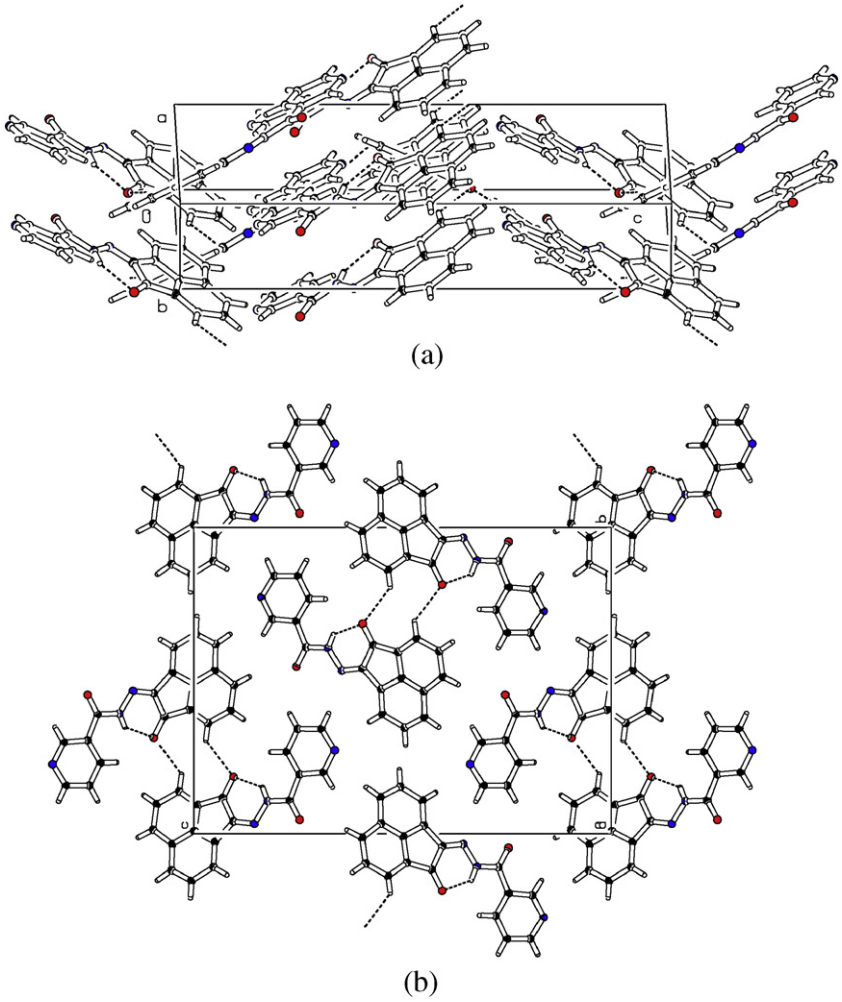

Fig. 5. Packing diagram of the molecules of polymorph II in the crystallographic unit cell. The view shown in the b) panel is a projection down the *a*-axis. The intra- and inter-molecular hydrogen bonds are shown as dotted lines.

packing of both polymorphs are depicted in Figs. 4, 5a and b. Other weak intermolecular interactions, such as those involving the π electron clouds as donors towards neighbor carbonyl atoms may also play a role in stabilizing the crystalline structure, in particular in polymorph I where the molecular stacking has a geometry suitable for such interaction (Fig. 6).

3.2. IR and Raman spectroscopies

The IR spectra, measured in attenuated total reflection (ATR) mode on single crystals of polymorphs I and II are shown in Fig. 7a. Additional FT-IR measurements in KBr pellets are given in supplementary material.

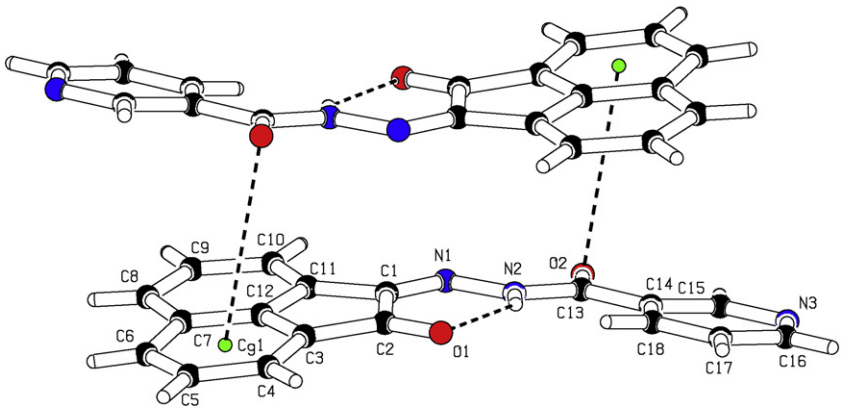

Fig. 6. Intermolecular interaction of the type $\pi\cdots O$ in polymorph I.

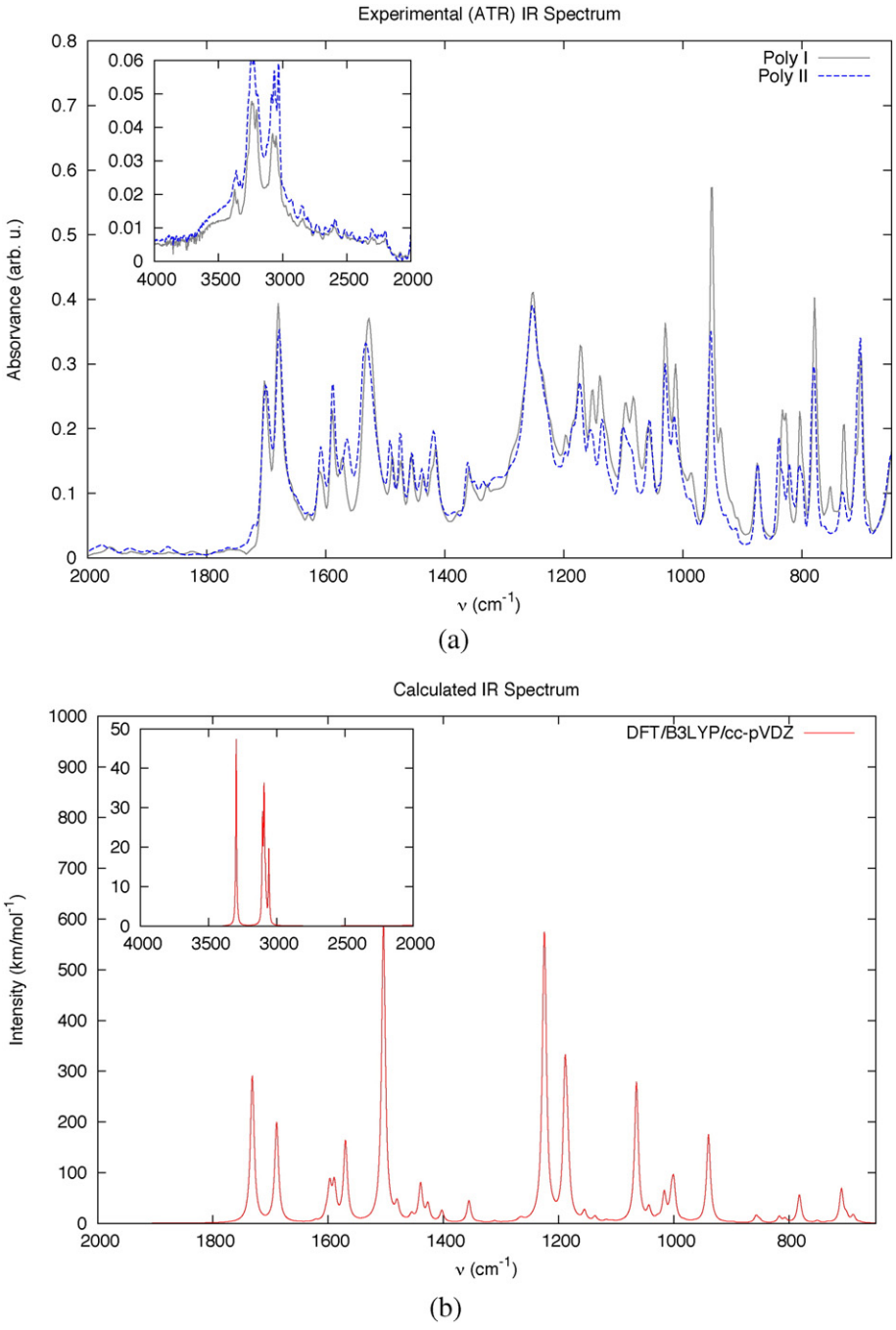

Fig. 7. a) ATR (Ge tip) Infrared spectrum of polymorphs I and II. b) Calculated DFT/B3LYP spectrum, with lines convoluted with a lorentzian profile of 4 cm^{-1} FWHM.

Herein, we focus our attention in the characteristic amide bands (I, II and III) observed by the presence of the acylhydrazones [20,21]. The assignment of these bands was performed based on previously reported studies [20–24] and supported by the analysis of the vibrational modes contributing to the lines of the calculated DFT/B3LYP IR spectrum (Table 6).

In amines, the NH stretching vibrations occur in the region 3500–3100 cm^{-1}. The broad band observed at 3244 cm^{-1} in the spectrum is assigned to the NH stretching mode, overlapped with aromatic CH stretching vibrations of the naphthyl and pyridyl rings. The appearance of well-defined vibrational bands between 1650 and 1500 cm^{-1} in the spectrum clearly supports that the ligand exists in the keto form. A strong band at 1678 cm^{-1} in the spectrum was assigned to the amide I band, originating mainly from the $\nu(C=O)$ group as well as from the $\nu(CN)$ stretching and $\delta(NH)$ bending, to a lesser extent. The strong band observed at 1701 cm^{-1} is due to the additional carbonyl group in the molecular structure. The intense amide II band located at 1533 cm^{-1} is due to the NH deformation with a $\nu(N-C=O)+\delta(NH)$ contribution. The CN vibration bands are more difficult to assign because these bands appear in the same range as the aromatic C═C and C–C stretching vibrations; however we have assigned the $\nu(CN)+\delta(NH)$ as the weak amide III band at 1362 cm^{-1}. Another $\nu(CC+CN)$ bands corresponding to the pyridyl ring were assigned at 1589, 953 and 702 cm^{-1}. Stretching mode of

Table 6
FT-IR and Raman intensities and assignment of vibrational modes. The calculated values are those provided by DFT/B3LYP using cc-pVDZ basis set, the wavenumbers having been scaled by the factor 0.970. Symbols used for classification of modes: *s*: stretching, *b*: bending, *o*: ooping, *w*: wagging, *skl*: skeleton.

$\bar{\nu}_{obs.}$ (cm^{-1})	$\bar{\nu}_{calc.}$ (cm^{-1})	IR intensity	Raman intensity	Mode
	583.0	1.12	28.87	$\nu_w C3=O2$
	677.6	1.16	12.90	$\nu_{skl}(acenaph)$
	688.7	14.29	3.24	$\nu_o N2-H$
	700.7	11.97	3.18	$\nu_w(pyr)$
702	709.2	66.02	7.44	$\nu_o C_{aryl}-H(acenaph)$
781s	782.3	54.76	0.98	$\nu_o C_{aryl}-H(acenaph)$
	785.4	1.52	17.28	$\nu_w C_{aryl}(acenaph)$
	817.3	12.09	3.28	$\nu_o C_{aryl}-H(pyr)$
	857.3	14.02	14.74	$\nu_s extended$
	897.7	1.54	51.15	$\nu_{skl}(acenaph)$
953m	940.1	172.10	1.66	$\nu_{skl}(acenaph)$
	1000.3	68.25	37.25	$\nu_w(pyr)$
	1004.1	40.03	15.88	$\nu_{skl}(acenaph)$
	1016.8	54.54	19.19	$\nu_s extended$
	1028.5	4.88	14.33	$\nu_s extended$
1057w	1043.3	24.88	61.46	$\nu_s extended$
1101s	1065.0	276.34	34.33	$\nu_s C1-N2+\nu_{skl}(acenaph)$
	1136.9	9.67	10.12	$\nu_s C1-N1+\nu_{skl}(acenaph)$
	1155.4	19.19	25.36	$\nu_s C1-N1+\nu_{skl}(acenaph)$
1136m	1184.5	99.85	22.60	$\nu_w(pyr)$
1173s	1188.9	280.99	118.83	$\nu_s N1-N2$
1254s	1223.9	322.40	359.65	$\nu_s N1-N2+\nu_b N2-H$
	1225.8	284.95	237.22	$\nu_s C13-C14$
	1264.0	3.88	189.67	$\nu_s C1-N1+\nu_{skl}(acenaph)$
	1268.0	4.14	41.26	$\nu_{skl}(pyr)$
1362w	1355.8	43.19	52.82	$\nu_s C1-N1+\nu_{skl}(acenaph)$
	1402.8	22.48	48.63	$\nu_{skl}(pyr)$
	1427.0	32.97	112.14	$\nu_s C1-N1+\nu_{skl}(acenaph)$
1419m	1439.6	74.33	76.18	$\nu_s C1-N1+\nu_{skl}(acenaph)$
1439w	1455.1	12.56	19.95	$\nu_{skl}(pyr)$
1475w	1480.4	31.34	24.99	$\nu_s C1-N1+\nu_{skl}(acenaph)$
1533s	1504.1	591.45	14.80	$\nu_b N2-H$
	1568.7	7.38	23.56	$\nu_{skl}(pyr)$
1589s	1570.1	151.97	2423.54	$\nu_s C1-N1$
	1589.3	68.89	214.81	$\nu_s C18-C17, C15-N3$
1608m	1597.3	67.94	63.08	$\nu_s C1-N1+\nu_{skl}(acenaph)$
	1603.5	11.12	635.53	$\nu_{skl}(acenaph)$
	1621.9	2.77	82.51	$\nu_{skl}(acenaph)$
1678s	1689.4	198.16	13.26	$\nu_s C2=O1$
1701s	1731.7	290.45	451.50	$\nu_s C13=O2$
3032w	3058.1	18.81	214.28	$\nu_s C_{aryl}(pyr)-H$
	3075.8	2.27	67.58	$\nu_s C_{aryl}(naph)-H$
	3078.5	1.06	83.41	$\nu_s C_{aryl}(naph)-H$
	3083.7	9.23	54.70	$\nu_s C_{aryl}(pyr)-H$
	3090.7	1.56	57.68	$\nu_s C_{aryl}(pyr)-H$
	3091.8	10.39	199.49	$\nu_s C_{aryl}(naph)-H$
3064w	3094.0	22.24	280.83	$\nu_s C_{aryl}(naph)-H$
	3103.9	10.09	191.98	$\nu_s C_{aryl}(pyr)-H$
	3104.9	12.94	279.62	$\nu_s C_{aryl}(naph)-H$
	3108.2	4.80	167.55	$\nu_s C_{aryl}(naph)-H$
3244w	3297.8	47.40	447.66	$\nu_s N2-H$

the C–N bond and stretching vibrations of the aromatic rings contribute to a band of moderate intensity at 1608 cm^{-1}. The deformation of the NH group produces a strong broad band observed at 1254 cm^{-1}. The most notorious differences of the IR spectra of the two polymorphs are seen in a line at 937 cm^{-1} clearly observed in form I but very weak in form II and, in the intensities of the peaks around 822 cm^{-1} and in the presence of a smaller but well defined peak at 752 cm^{-1} in form I that is almost absent in form II.

The Raman spectra of the two polymorphs are shown in Fig. 8a to be compared to that of the free molecule given by the DFT/B3LYP calculations, depicted in Fig. 8b. The Raman spectra were obtained with relatively short acquisition times (15 scans of 3.8 s @5 mW and 20 scans of 11 s @1 mW for polymorphs I and II, respectively) as the crystals were found to rapidly deteriorate under the laser beam. A 100× objective lenses was used giving a spot diameter of 0.8 μm. Again, differences of the relative intensities of a few bands distinguish the two polymorphs.

3.3. Ab-initio and DFT calculations

In order to better disclose the role of intermolecular interactions in determining the conformation of the molecule observed in the two polymorphs we have performed quantum chemistry calculations of the geometry of the free molecule using both *ab-initio* Hartree–Fock and Density Functional Theory methods. The starting geometry for geometry optimization was that measured in the crystal (polymorph I). The optimization was performed with tight conditions on the SCF energy convergence and residual energy gradient, and at the end of the procedure the Hessian matrix was checked for the presence of any imaginary component and none was found. We have also checked that the found minimum is the global energy minimum in the conformation space of the molecule, by systematically scanning the relevant torsion angles. Interestingly, for small basis sets (3-21G) the calculated equilibrium geometry of the free molecule is planar. However, use of extended basis sets reproduced the non-planar geometry with values of α and β torsion angles close to those observed in polymorph II. Best agreement was achieved with DFT/B3LYP/cc-pVDZ (Table 4). The torsion angle ϵ is calculated close to zero, differing from the observed values in the crystal, therefore we conclude that this torsion angle is affected by interactions in the crystal. Many features of our calculations, in particular concerning the geometry and electrostatic potential of the acenaphthenequinone moiety are in agreement with the findings of a similar DFT study recently reported on a carbonyl acenaphthenequinone derivative [25]. The calculation of the vibrational IR and Raman spectra was performed after geometry optimization for the DFT/B3LYP/cc-pVDZ method and, after proper convolution with instrumental resolution, they were used for comparison with the measured spectra.

3.4. UV–vis spectroscopy

The UV–vis absorption was measured in CH_3CN at room temperature. The measured spectrum, compared to those of acenaphthenequinone and nicotinic hydrazide is shown in Fig. 9a. The compound exhibits a band around 264 nm assignable to the aromatic $\pi \rightarrow \pi^*$ transitions of the acenaphthenequinone. The intense broad band observed at 322 nm can be assigned to the $n \rightarrow \pi^*$ type electronic transitions [23]. Further, deconvolution of low-energy bands, overlapped in the zone 350–500 nm, was performed by a fit to a sum of Gaussian functions as shown in Fig. 9b. Four low-energy bands are centered at positions 354, 415, 440 and 476 nm, respectively. Our TDDFT calculations for the molecule in acetonitrile (solvent effects included as C-PCM/SMD model) of the 25 lower energy singlet excitations give a good qualitative description of the observed UV–vis spectrum. The most intense calculated electronic transitions occur as a close doublet at 323/328 nm and an intense high energy transition is calculated also as a close doublet at 236/241 nm. Four lower energy transitions with smaller intensity were calculated in the range 334–420 nm, the lowest energy corresponding to the HOMO–LUMO transition.

3.5. NMR

In order to contribute some information about the behavior of the compound in solution, the ^1H and ^{13}C NMR spectra were recorded using DMSO-d_6. The use of two-dimensional spectra (provided as Supplementary materials S3 and S4), COSY (correlation spectroscopy), HMQC (heteronuclear multiple quantum correlation) and

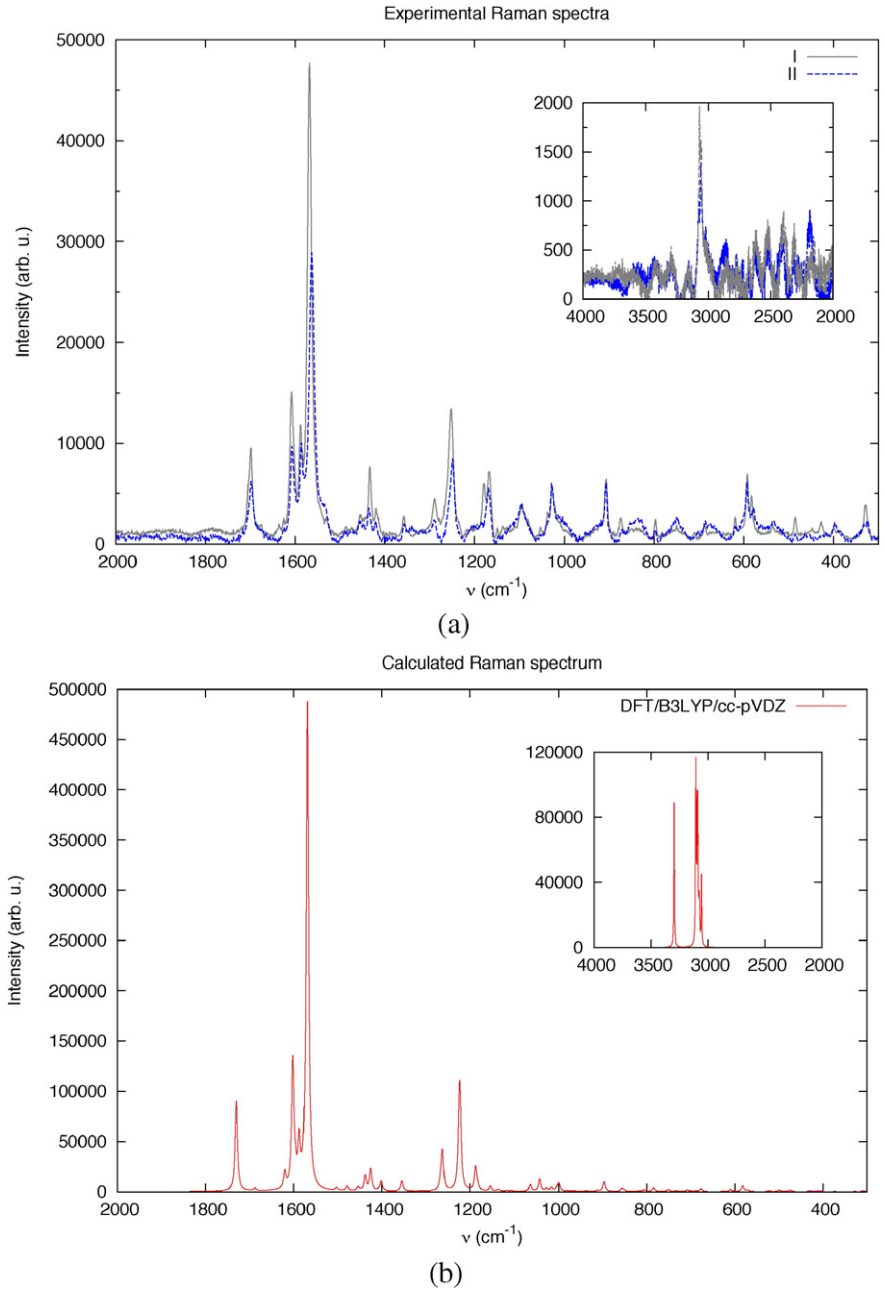

Fig. 8. Experimental (a) and calculated (b) Raman spectra. The inset shows the high frequency range of the spectra.

HMBC (heteronuclear multiple bond correlation) experiments have allowed a full assignment in Table 7. ^{1}H NMR signal of the N2H proton appears at 12.02 ppm possibly due to hydrogen bond formation between solvent molecules and amide proton [24]. Two signals for each proton are observed in the region 9.14–7.64 ppm caused by the presence of *E*, *Z* isomers with a higher extent in the *E* form [24] (Figs. S3–S4). The corresponding number of protons was calculated from the sum of both signals (see Table 7). The signals in the region 8.52 − 7.62 ppm are assigned to the protons of pyridyl and naphthyl. Protons of C4, C5 and C9 appear as a multiplet at 7.98–7.85 ppm, for which the calculated integral signal agrees with the presence of three hydrogen atoms. In ^{13}C NMR, the signals corresponding to C2 and C13 carbonyl are at 188 and 156 ppm, respectively. The C1 signal shifts down around 10 ppm with respect to the values of another acylhydrazones from nicotinic hydrazide [1] probably because of the proximity of the C2 carbonyl atom.

4. Conclusions

A novel hydrazone, 2-oxoacenaphthylen-1(2*H*)-ylidene nicotinohydrazide has been synthesized and was found to crystallize in two polymorphs, with monoclinic and orthorhombic structures. The two polymorphs have been characterized by single-crystal X-ray diffraction that disclosed a distinct crystal packing of the molecules that slightly differ in their conformation, as result of distinct intermolecular interactions in the crystal. In fact, in addition to a common intramolecular hydrogen bond between the NH group and the carbonyl group, polymorph II features an additional weak intermolecular C − *H*···*O* hydrogen bond whereas in polymorph I interactions between the aromatic π electron clouds and the carbonyl atoms appear to be more relevant. The polymorphs were studied by spectroscopic techniques (FT-IR and Raman) aiming at finding in the vibrational spectra distinct signatures arising from the different

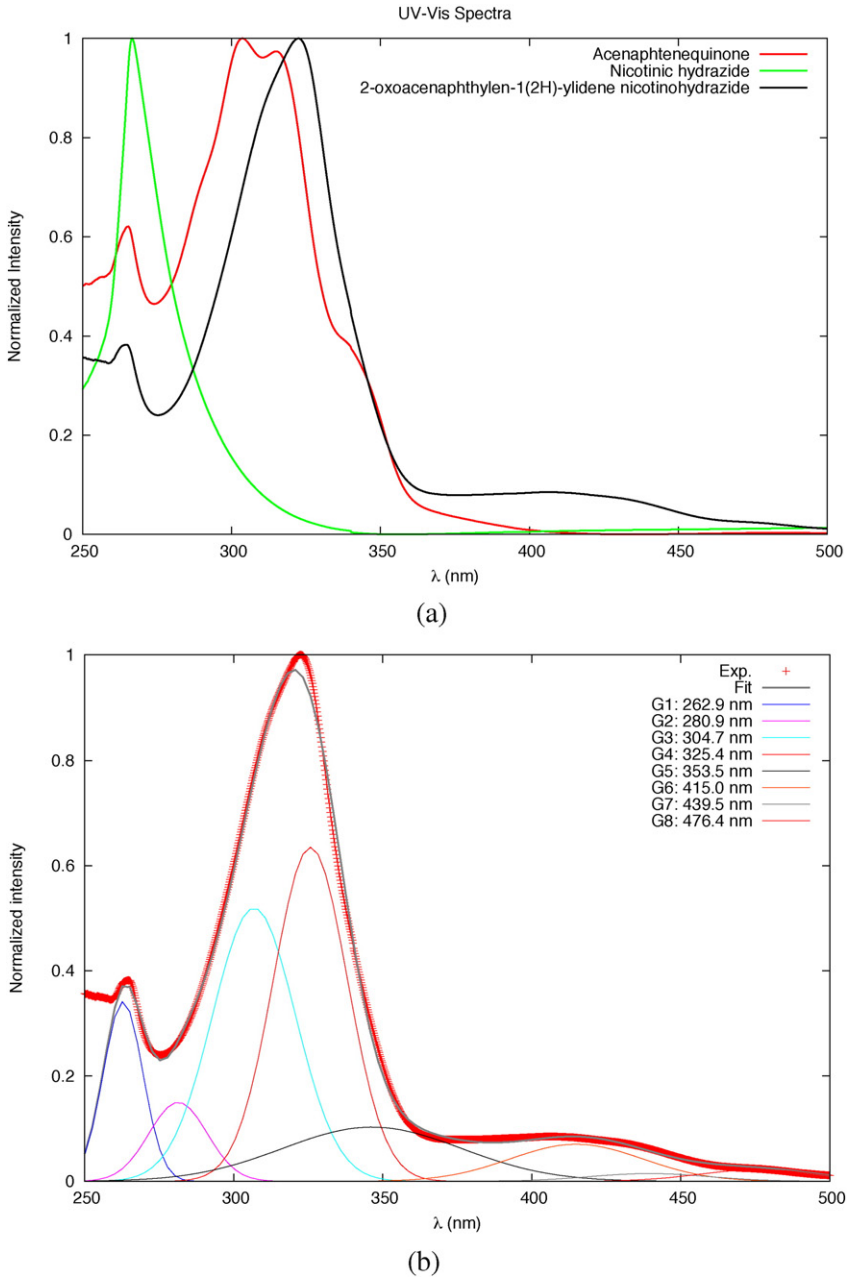

Fig. 9. UV absorption spectra of (a) of 2-oxoacenaphthylen-1(2*H*)-ylidene nicotinohydrazide and the reactants acenaphthenequinone and nicotinic hydrazide and (b) deconvolution of absorption peaks in the compound using Gaussian functions.

intermolecular interactions. To better interpret the spectra, *ab-initio* HF and DFT calculations were performed on the isolated molecule. These calculations reproduce well the molecular geometry observed in the crystal, with torsion angles closer to those found in the conformation of polymorph II. The vibrational spectra of the two polymorphs are similar but show subtle differences in the intensities of a few absorption bands that can be used to identify the polymorphs. NMR studies in solution (DMSO-d_6) showed the presence of the two tautomeric *E*/*Z* forms, the *E* form that is observed in the crystals being also predominant in solution.

Acknowledgments

Access to TAIL-UC facility funded under QREN-Mais Centro project ICT 2009_02_012_1890 and to the Coimbra LaserLab funded under grant number 228334 of the European Community 7th Framework program is gratefully acknowledged. The authors are also grateful to Prof.

Table 7
^{1}H NMR and ^{13}C NMR spectra data (δ, ppm; *J*, Hz).

^{1}H NMR		
E form	*Z* form	Int
12.02 (s, N2H)		
9.14 (d, $J = 2.0$, C15H)	9.18 (d, $J = 2.0$, C15H)	1
8.88 (dd, $J = 4.4$, $J' = 1.0$, C16H)	8.84 (dd, $J = 4.5$, $J' = 1.2$, C16H)	1
8.45 (d, $J = 8.1$, C10H)	8.52 (d, $J = 5.6$, C10H)	1
8.34 (dt, $J = 8.1$, $J' = 1.8$, C18H)	8.39 (d, $J = 7.9$, C18H)	1
8.22 (d, $J = 8.2$, C6H)	8.26 (d, $J = 8.4$, C6H)	1
8.17 (d, $J = 7.0$, C8H)	8.11 (d, $J = 6.9$, C8H)	1
7.98–7.85 (m, C4H/C5H/C9H)	7.98–7.85 (m, C4H/C5H/C9H)	3
7.69 (dd, $J = 7.7$, $J' = 4.7$, C17H)	7.64 (dd, $J = 8.4$, $J' = 5.3$, C17H)	1

^{13}C NMR (*E*,*Z* forms).
188.6/188.2 (C2), 156.1/156.0 (C13), 155.3/155.2 (C1), 138.8/138.4 (C16). 136.8/136.6 (C15), 132.7/132.0 (C10), 130.9/130.1 (C3/C7/C11/C12/C14/C18), 129.9/128.9 128.5/128.3 (C4-C5), 127.7/126.4 (C6), 123.1/123.0 (C17), 122.2/121.7 (C8), 117.6/177.6 (C9).

Rui Fausto (Department of Chemistry, University of Coimbra) for the help with the ATR IR spectroscopy measurements and CACTI, Universidade de Vigo, for technical support.

Appendix A. Supplementary data

CCDC 1411972 (polymorph I) and CCDC 1411973 (polymorph II) contain the supplementary crystallographic data. These data can be obtained free of charge from The Cambridge Crystallographic Data Centre via http://www.ccdc.cam.ac.uk/data_request/cif. Supplementary data associated with this article can be found, in the online version at http://dx.doi.org/10.1016/j.saa.2016.02.012.

References

[1] D. Rogolino, M. Carcelli, A. Bacchi, C. Campari, L. Contardi, E. Fisicaro, A. Gatti, M. Sechi, A. Stewart, L. Naesens, A versatile salicyl hydrazonic ligand and its metal complexes as antiviral agents, J. Inorg. Biochem. 150 (2015) 9–17.
[2] G. Turan-Zitouni, L. Yurttas, Z.A. Kaplancikli, Ö.D. Can, U.D. Özkay, Synthesis and anti-nociceptive, anti-inflammatory activities of new aroyl propionic acid derivatives including *N*-acylhydrazone motif, Med. Chem. Res. 6 (2015) 2406–2416.
[3] T.F. Silva, W. Bispo, M. Alexandre-Moreira, F.N. Costa, C.E. Monteiro, F.F. Ferreira, R.C. Barroso, F. Noël, R.T. Sudo, G. Zapata-Sudo, L.M. Lima, E.J. Barreiro, Novel orally active analgesic and anti-inflammatory cyclohexyl-*N*-acylhydrazone derivatives, Molecules 20 (2015) 3067–3088.
[4] L. Xia, Y. Xia, L. Huang, X. Xiao, H.Y. Lou, T.J. Liu, W.D. Pan, H. Luo, Benzaldehyde schiff bases regulation to the metabolism, hemolysis, and virulence genes expression in vitro and their structure and microbicidal activity relationship, Eur. J. Med. Chem. 97 (2015) 83–93.
[5] X. Su, I. Aprahamian, Hydrazone-based switches, metallo-assemblies and sensors, Chem. Soc. Rev. 43 (6) (2014) 1963–1981.
[6] L. Mazur, K.N. Jarzembska, R. Kaminski, K. Wozniak, E. Pindelska, M. Zielinska-Pisklak, Substituent and solvent effects on intermolecular interactions in crystals of *N*-acylhydrazone derivatives: single-crystal X-ray, solid-state NMR, and computational studies, Cryst. Growth Des. (2014) 2263–2281.
[7] N. Mathew, M. Sithambaresan, M.R.P. Kurup, Spectral studies of copper(II) complexes of tridentate acylhydrazone ligands with heterocyclic compounds as coligands: X-ray crystal structure of one acylhydrazone copper(II) complex, Spectrochim, Acta Mol. Biomol. Spectrosc. 79 (5) (2011) 1154–1161.
[8] M.C. Rodríguez-Argüelles, S. Mosquera-Vazquez, P. Tourón-Touceda, J. Sanmartín-Matalobos, A. García-Deibe, M. Belicchi-Ferrari, G. Pelosi, C. Pelizzi, F. Zani, Complexes of 2-thiophenecarbonyl and isonicotinoyl hydrazones of 3-(*N*-methyl)isatin. A study of their antimicrobial activity, J. Inorg. Biochem. 101 (2007) 138–147.
[9] Bruker AXS Inc., APEX2, SAINT and SADABS, Madison, Wisconsin, USA, 2006.
[10] G.M. Sheldrick, SHELXT-integrated space-group and crystal-structure determination, Acta Crystallogr. A71 (2015) 3–8.
[11] G.M. Sheldrick, Crystal structure refinement with SHELXL, Acta Crystallogr. C71 (2015) 3–8.
[12] A. Spek, Structure validation in chemical crystallography, Acta Crystallogr. D65 (2009) 148–155.
[13] T.H. Dunning, Gaussian basis sets for use in correlated molecular calculations. I. The atoms boron through neon and hydrogen, J. Chem. Phys. 90 (2) (1989) 1007–1023.
[14] M.W. Schmidt, K.K. Baldridge, J.A. Boatz, S.T. Elbert, M.S. Gordon, J.H. Jensen, S. Koseki, N. Matsunaga, K.A. Nguyen, S.J. Su, T.L. Windus, M. Dupuis, J.A. Montgomery, General atomic and molecular electronic structure system, J. Comput. Chem. 14 (1993) 1347–1363.
[15] NIST, Computational chemistry comparison and benchmark database, http://cccbdb.nist.gov/vibscalejust.asp.
[16] A.V. Marenich, C.J. Cramer, D.G. Truhlar, Universal solvation model based on solute electron density and on a continuum model of the solvent defined by the bulk dielectric constant and atomic surface tensions, J. Phys. Chem. B 113 (2009) 6378–6396.
[17] Y. Chan, A. Salhin, M. Ali, M. Khairuddean, B. Salleh, Synthesis, crystal structure and antimicrobial activity of (*E*)-ethyl-4-(2-oxoacenaphthylen-1(2H)-ylideneamino) benzoate, J. Crystal. Process. Technol. 3 (2013) 69–73.
[18] J. Zhou, H. Sun, K. Harms, J. Sundermeyer, Synthesis and X-ray crystal structures of acenaphthenequinone-based α-diimine palladium complexes and a novel V-shape tripalladium cluster, Z. Anorg. Allg. Chem. 634 (9) (2008) 1517–1521.
[19] M.C. Rodríguez-Argüelles, M.B. Ferrari, G.G. Fava, C. Pelizzi, G. Pelosi, R. Albertini, A. Bonati, P.P. Dall'Aglio, P. Lunghi, S. Pinelli, Acenaphthenequinone thiosemicarbazone and its transition metal complexes: synthesis, structure, and biological activity, J. Inorg. Biochem. 66 (1997) 7–17.
[20] J.R. Anacona, M. Rincones, Tridentate hydrazone metal complexes derived from cephalexin and 2-hydrazinopyridine: synthesis, characterization and antibacterial activity, Spectrochim. Acta Mol. Biomol. Spectrosc. 141 (2015) 169–175.
[21] J. Benítez, C.D. Queiroz, I. Correia, M.A. Amaral, M.S. Alexandre-Moreia, E.J. Barreiro, L.M. lima, J. Varela, M. González, H. Cerecetto, V. Moreno, J.C. Pessoa, D. Gambino, New oxidovanadium(IV) N-acylhydrazone complexes: promising antileishmanial and antitrypanosomal agents, Eur. J. Med. Chem. 62 (2013) 20–27.
[22] N. Hosny, Synthesis and spectroscopic studies of (*E*)- *N*–(1-phenylethylidene) nicotinohydrazide (PNH) and some of its metal complexes, J. Mol. Struct. 923 (1–3) (2009) 98–102.
[23] R. Gup, C. Gökçe, S. Aktürk, Copper(II) complexes with 4-hydroxyacetophenone-derived acylhydrazones: synthesis, characterization, DNA binding and cleavage properties, Spectrochim, Acta Mol. Biomol. Spectrosc. 134 (2015) 484–492.
[24] N. Galic, I. Brodanac, D. Kontrec, S. Miljanic, Structural investigations of aroylhydrazones derived from nicotinic acid hydrazide in solid state and in solution, Spectrochim. Acta Mol. Biomol. Spectrosc. 107 (2013) 263–270.
[25] L. Sinha, O. Prasad, V. Narayan, R.K. Srivastava, Electronic structure, non-linear properties and vibrational analysis of acenaphthene and its carbonyl derivative acenaphthenequinone by density functional theory, J. Mol. Struct. 958 (1–3) (2010) 33–40.